In-medium effects for nuclear matter in the Fermi-energy domain

O. Lopez,[1] D. Durand,[2] G. Lehaut,[2] B. Borderie,[2] J. D. Frankland,[3] M. F. Rivet,[4] R. Bougault,[4] A. Chbihi,[4] E. Galichet,[4] D. Guinet,[5] M. La Commara,[6] N. Le Neindre,[7] I. Lombardo,[7] L. Manduci,[7] P. Marini,[8] P. Napolitani,[8] M. Pârlog,[8] E. Rosato,[8] G. Spadaccini,[8] E. Vient,[8] and M. Vigilante[8]
(INDRA Collaboration)
[1]*Laboratoire de Physique Corpusculaire, ENSICAEN, Université de Caen Basse Normandie, CNRS/IN2P3, F-14050 Caen Cedex, France*
[2]*Institut de Physique Nucléaire, CNRS/IN2P3, Université Paris-Sud 11, F-91406 Orsay Cedex, France*
[3]*Grand Accélérateur National d'Ions Lourds, CEA/DSM-CNRS/IN2P3, B.P. 5027, F-14076 Caen Cedex, France*
[4]*Conservatoire National des Arts et Métiers, F-75141 Paris Cedex 03, France*
[5]*Institut de Physique Nucléaire, CNRS/IN2P3, Université Claude Bernard Lyon-1, F-69622 Villeurbanne Cedex, France*
[6]*Dipartimento di Scienze Fisiche e Sezione INFN, Università di Napoli "Federico II", I-80126 Napoli, Italy*
[7]*EAMEA, CC19 50115 Cherbourg-Octeville Cedex, France*
[8]*Centre d'Études Nucléaires de Bordeaux-Gradignan, CNRS/IN2P3 - Université de Bordeaux I, F-33175 Gradignan Cedex, France*
(Received 2 September 2014; revised manuscript received 31 October 2014; published 1 December 2014)

Background: By looking specifically at free nucleons (here protons), we present for the first time a comprehensive body of experimental results concerning the mean free path, the nucleon-nucleon cross-section and in-medium effects in nuclear matter.
Purpose: Using the large dataset of exclusive measurements provided by the 4π array *INDRA*, we determine the relative degree of stopping as a function of system mass and bombarding energy. We show that the stopping can be directly related to the transport properties in the nuclear medium.
Methods: We perform a systematic study of protons nuclear stopping in central collisions for heavy-ion induced reactions in the Fermi-energy domain, between 15A and 100A MeV.
Results: It is found that the mean free path exhibits a maximum at $\lambda_{NN} = 9.5 \pm 2$ fm, around $E_{\rm inc} = 35A$–$40A$ MeV incident energy and decreases toward an asymptotic value $\lambda_{NN} = 4.5 \pm 1$ fm at $E_{\rm inc} = 100A$ MeV.
Conclusions: After accounting for Pauli blocking of elastic nucleon-nucleon collisions, it is shown that the effective in-medium NN cross section is further reduced compared to the free value in this energy range. Therefore, in-medium effects cannot be neglected in the Fermi-energy range. These results bring new fundamental inputs for microscopic descriptions of nuclear reactions in the Fermi-energy domain.

DOI: 10.1103/PhysRevC.90.064602 PACS number(s): 25.70.−z, 21.65.Mn

I. INTRODUCTION

Transport properties in nuclear matter contribute to the determination of the equation of state via the underlying in-medium properties of the nuclear interaction and are one of the fundamental ingredients for microscopic models [1–9]. They are also critical in the description of the supernova core collapse and the formation of a neutron star [10]. These properties can be probed with the help of heavy-ion induced collisions (HIC) by looking at dissipation phenomena in terms of energy and isospin transport and thus related to the stopping. In the Fermi-energy domain, transport features should exhibit the interplay between mean-field (nuclear degrees of freedom) and individual (nucleonic degrees of freedom) effects, especially when looking at the energy dissipation reached in central collisions [11].

From a theoretical point of view, the knowledge of the dissipation mechanism for nuclear matter in HIC is related to the properties of the mean-field itself via the one-body dissipation (nuclear friction and viscosity) and nucleon-nucleon (NN) collisions via two-body dissipation in the nuclear medium. In the studied energy range, below 100A MeV, only NN elastic channels must be considered. At low incident energy, i.e., lower than the Fermi energy, where mean-field effects prevail, NN collisions are strongly suppressed due to the fermionic nature of nucleons, known as Pauli blocking. At high incident energy, while the available space for NN collisions increases, the situation is the opposite since the mean field becomes less and less attractive while NN collisions become important [12–14]. Then, one expects the in-medium NN cross section to be very small at low incident energy and to become sizable (asymptotically approaching the *free* NN cross section) as the incident energy becomes significantly higher than the Fermi energy. In this framework, one may wonder what is the magnitude of in-medium effects induced by many-body correlations in nuclear reactions. Numerous theoretical approaches show that the cross section has to be properly renormalized in order to account for the *effective* NN collision rate in HIC [15], and several effects must be considered. First, the Pauli blocking effect discussed above reduces the NN collision rate [12] and can be viewed as a "trivial" two-body correlation due the quantal nature of protons and neutrons. Higher-order correlations in NN collisions due to the high-density conditions encountered in central collisions [12,13,15] can also come into play, as shown in some theoretical works done in the past two decades [15–18]. They mainly use relativistic mean-field approaches with realistic (effective) nucleon-nucleon interactions. They conclude that the in-medium NN cross sections are isopin dependent, and have to be renormalized (reduced) in the nuclear medium as compared to free vacuum values. They show that the

 ©2014 American Physical Society

nucleon mean free path is large, typically larger than the nucleus size for $E_{\rm inc}/A \leqslant 100$ MeV, and decreases toward a saturation value $\lambda_{NN} = 4$–5 fm at high incident energy, for $E_{\rm inc}/A \geqslant 100$ MeV [18]. Thus, the situation at high energy, where the mean free path is supposed to be almost constant, is quite clear. This is not the case in the Fermi-energy domain; indeed, in-medium effects and especially quenching factors for the *NN* cross section are largely unknown in the range $E_{\rm inc}/A = 10$–100 MeV [19] and have to be constrained experimentally.

From an experimental point of view, nuclear stopping has been determined by the FOPI Collaboration for the Au+Au system in the incident energy range $90A$–$1930A$ MeV using several observables [6]. The study concluded that there is a broad plateau of maximal stopping between $200A$ and $800A$ MeV [6,20]. For the Fermi-energy domain, the situation is quite different. In our previous paper [11], we have shown that the stopping measured as the ratio between transverse and longitudinal energies of the reaction products can probe the energy dissipation in central collisions and shed light on the dissipation mechanism itself. A transition was observed from a one-body to a two-body dissipation mechanism as a function of the incident energy. The transition occurs around $35A$ MeV (close to the Fermi energy at saturation density), whatever the system size. It corresponds to a *minimal* value for the stopping [11]. These results call for an extended analysis of the experimental data. The purpose of this paper is then a continuation of this work, where we try to relate the observed dependence for the stopping in central collisions to the nucleon mean free path λ_{NN} and the corresponding cross section σ_{NN} in the nuclear medium.

II. EXPERIMENTAL CONSIDERATIONS

A. INDRA dataset

In this analysis, we use the full INDRA dataset for symmetric or nearly symmetric systems recorded along the past two decades at GANIL and GSI facilities. The experimental data are exclusive and correspond to a nearly complete detection of all charged products of the reaction thanks to the powerful INDRA 4π array [21]. Details concerning the data collection can be found in [22–27]. Table I shows some basic characteristics of the studied systems.

We note that the data cover a broad domain of incident energy, here from $15A$ up to $100A$ MeV, and concern 42 systems with a total mass between 72 and 476 mass units. Isospin is here between $N = Z$ and $N/Z \approx 1.6$. This constitutes, to our knowledge, the largest body of experimental data in the Fermi-energy domain covered with the same setup. Two systems in Table I are not fully symmetric (^{36}Ar+^{58}Ni and ^{155}Gd+^{238}U) but still present a small mass asymmetry; they have been taken in order to cover more efficiently the mass/energy domain of the analysis. In the following, we will display all quantities as a function of the incident energy in the laboratory frame. In a more general perspective, one should prefer to use the available center-of-mass energy, especially when including asymmetric systems.

TABLE I. Characteristics of the 42 (quasi)symmetric systems measured with INDRA and analyzed in this study. The mass asymmetry in the entrance channel is defined as Asym $= |A_{\rm projectile} - A_{\rm target}|/(A_{\rm projectile} + A_{\rm target})$. Numbers in brackets in the third column indicate the number of measured bombarding energy.

System	$A_{\rm tot}$ (amu)	$E_{\rm inc}$ (A MeV)	Asym	$(N/Z)_{\rm tot}$
^{36}Ar + KCl	72	32–74 (5)	0	1
^{36}Ar +^{58} Ni	94	32–95 (7)	0.23	1.04
^{58}Ni +^{58} Ni	116	32–90 (7)	0	1.07
^{129}Xe +^{129} Sn	248	15–100 (14)	0.04	1.39
^{181}Ta +^{197} Au	378	33, 40 (2)	0.04	1.49
^{197}Au +^{197} Au	394	40–100 (4)	0	1.49
^{155}Gd +^{238} U	393	36 (1)	0.21	1.59
^{208}Pb +^{197} Au	405	29 (1)	0.03	1.52
^{238}U +^{238} U	476	24 (1)	0	1.59

B. Event selection

In the following, we want to probe the degree of stopping in central collisions. We have then chosen to study the very dissipative collisions that produce the highest charged particle multiplicities M_{ch}; we use the multiplicity selection as a *minimum bias* selector. By doing so, we minimize the inevitable autocorrelations between the event selection and the observable of interest, here the isotropy ratio built upon the kinematical properties of particles. We use a scalar variable, M_{ch}, as event selector in order to look at a vector observable, namely the energy isotropy ratio R_E. This latter is defined on an event-by-event basis:

$$R_E = \frac{1}{2}\frac{\sum_i^N E_i^{\perp}}{\sum_i^N E_i^{\parallel}}, \tag{1}$$

where $E_i^{\perp}$ and $E_i^{\parallel}$ are the transverse and longitudinal center-of-mass (c.m.) energies for particle i. The summation is done over the total number N of (detected) reaction products in the selected event. By construction, R_E is equal to 1 for an isotropic emission, <1 for an elongated emission along the longitudinal direction given by the beam direction, and >1 for preferential emission in the plane transverse to the beam direction. Since we are looking at INDRA data, the sum is restricted to charged products only, however we benefit from the excellent 4π coverage of the experimental apparatus. Figure 1 presents the correlation between the charged particle multiplicity M_{ch} and the isotropy ratio R_E obtained from INDRA data for the four Xe+Sn systems at $15A$, $25A$, $39A$, and $65A$ MeV. The INDRA trigger was set to $M_{ch} > 3$, allowing us to record 60–80% of the total reaction cross section [11]. The M_{ch} bins have been normalized to the same number of entries in order to reduce the statistical fluctuations as done in [11]. The black histograms are the corresponding mean R_E values.

This correlation presents a saturation at the highest multiplicity values, represented by the black histogram in Fig. 1. We then define a multiplicity cut in order to retain the events corresponding to $M_{ch} > M_{ch}^{cut}$, visible as the symbols onto Fig. 1. The multiplicity cut clearly depends on the system and has been set using the same strategy for the whole dataset

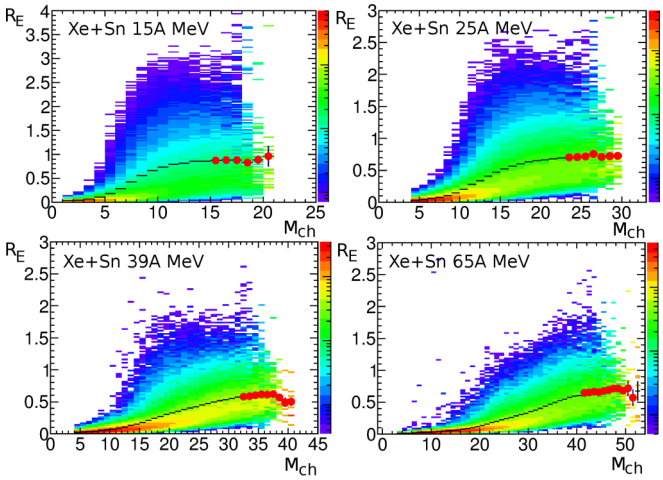

FIG. 1. (Color online) Isotropy ratio R_E as a function of total charged multiplicity M_{ch} for Xe+Sn at 15A, 25A, 39A, and 65A MeV. The black histograms show the mean values and the grey (red) symbols indicate the event selection. All M_{ch} bins have been normalized to the same number of entries.

of Table I. The selection retains typically between 50 and 150 mb, thus corresponding, assuming that only the most central collisions are selected, to an impact parameter range between 0 and $b = 1$–1.5 fm (i.e., 1–2% of the detected events). Alternatively, we could have used a fixed value of the total cross section for all systems (for example the lowest one, 50 mb), but this would not change substantially the results concerning the extracted R_E values.

C. Particle selection

In order to probe the nucleon properties in nuclear medium, we have to focus specifically on free nucleons. They indeed carry genuine information about NN collisions, i.e., out of any coalescence phase and without clusterization into fragments occurring during the course of the collision [28].

In Fig. 2, we can see the c.m. velocity plots in invariant cross section for protons (left) and α particles (right), for the selected central events for the ^{129}Xe+^{124}Sn system at 65A MeV. Protons clearly exhibit different kinematical features compared to α particles, with a strong emission located at midrapidity

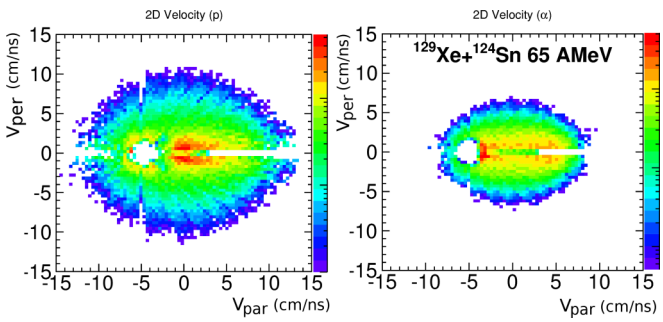

FIG. 2. (Color online) c.m. transverse versus parallel velocities for protons (left) and α particles (right) in invariant cross section, for the selected central events of the ^{129}Xe+^{124}Sn system at 65A MeV.

and an extension to high transverse velocities suggesting a nonequilibrium emission. We will then consider that protons are predominantly produced before thermalization of the produced hot nuclei and not from secondary decay as already seen in a previous study for Xe+Sn central collisions [25].

In the following, we limit our study to protons, for which we compute the isotropy ratio R_E and call it hereafter R_E^p. To avoid the statistical fluctuations coming from the event-by-event determination of R_E^p, we instead compute the isotropy ratio from the *full* set of protons selected by the multiplicity cut, considering thus all protons detected in these events as though they are coming from a single event. It is worthwhile to note that this procedure weakly lowers (5–10%) the mean values for R_E^p as compared to the event-by-event determination.

III. STOPPING IN NUCLEAR MATTER

A. Stopping ratio for protons

Applying the protocol presented in the previous section, we compute the isotropy ratio R_E^p for the 42 different systems listed in Table I. The results are presented in Fig. 3 as a function of the incident energy.

The error bars in Fig. 3 correspond to the statistical errors supplemented by an estimate of the systematic errors coming from the experimental determination for R_E^p. For these latter, we use the same prescription as in [11]: we consider here a "reasonable" variation for the multiplicity cuts $M_{ch}^{cut} \pm 1$ in the event selection and take the corresponding R_E^p intervals as an estimator of the systematic errors. They are found to contribute to more than half of the total error bars, depending on systems. In the following, the error bars displayed on all computed quantities will derive from these ones, and thus will incorporate not only statistical but also (some) systematic errors.

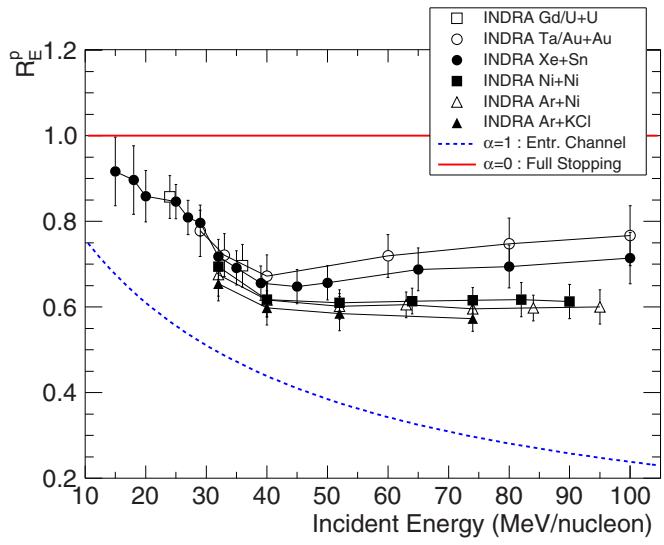

FIG. 3. (Color online) Mean isotropy ratio for protons R_E^p as a function of energy. The symbols represent the different studied systems. The lower dashed curve represents the expected value for the entrance channel (no stopping) and the upper straight line for the full stopping.

We now compare the results for R_E^p to the ones obtained for R_E in [11] for all particles (no proton selection). Although the values are systematically higher, we find a similar behavior: a quite steep decrease from low incident energy to Fermi energy followed by a flattening or even a modest increase for the isotropy ratio at higher incident energies. We also get a similar mass scaling for the different systems: the heavier the system, the higher the isotropy ratio is. This supports the fact that the stopping, i.e., the conversion from longitudinal to transverse energy, is related to the number of participants in the system as in a *Glauber* description of the collision [29]. The difference with [11] comes from the location in incident energy of the transition between the two regimes; it is $30A$–$35A$ MeV in [11] while it is slightly above in the present study, between $35A$ and $40A$ MeV. We can also notice that the mean isotropy ratio is always below 1 and thus on average the proton momentum distribution never achieves the isotropy which we associate with full stopping for the selected events. This was also the case in [11].

To get more quantitative values for the stopping, the isotropy ratio is compared to two extreme values. They are computed by assuming two *Fermi* spheres in p-space separated by the relative momentum corresponding to $E_{\rm inc}$, which is the incident energy and α a parameter equal to 1 for complete transparency (no dissipation, lower dashed curve in blue) and 0 for full stopping (upper straight line in red). A straightforward calculation for the isotropy ratio $R_E(\alpha)$ can be obtained analytically:

$$R_E(\alpha) = \frac{1}{1 + 5\alpha x/4} \tag{2}$$

where $x = E_{\rm inc}/E_{\rm Fermi}$ and $E_{\rm Fermi} = 38$ MeV is the Fermi energy at saturation density. An estimate for the stopping reached in our dataset of central events is then given by the normalized quantity $\mathcal{S}$, called hereafter stopping ratio, as

$$\mathcal{S} = \frac{R_E^p - R_E(\alpha = 1)}{R_E(\alpha = 0) - R_E(\alpha = 1)}. \tag{3}$$

This quantity is always positive since $R_E^p > R_E(\alpha = 1)$ and $R_E(\alpha = 0) > R_E(\alpha = 1)$.

Figure 4 displays the stopping ratio $\mathcal{S}$ (in percentage) and emphasizes the location of the minimal stopping value around $40A$ MeV, together with the two different regimes for dissipation. As expected from Fig. 3, we find stopping ratio values ranging between 0 and 1. The minimum stopping, $\mathcal{S}_{\rm min} = 20$–$35\%$, depends on the system. It is larger for the heavier systems ($\mathcal{S}_{\rm min} \approx 35\%$), here Ta/Au+Au and U+U. Let us recall that R_E^p is larger than R_E. We attribute this effect to the fact that free nucleons, supposedly *NN* collisions, have to be emitted *outside* the two nuclei in p-space. We are going to develop this point in the next section.

B. Stopping ratio and NN collisions

In this section, we want to link the stopping ratio $\mathcal{S}$ to a quantity related to the amount of *NN* collisions, taking into account the proper available phase space in momentum. To do so, we use a simple Monte Carlo simulation, taking again the two Fermi spheres described in the previous section, and we implement elastic *NN* collisions in a semiclassical way; to perform such collisions, we pick randomly one nucleon from the projectile and one from the target and rotate the corresponding momenta around their own c.m. frame. In this procedure, we do not consider multiple scatterings nor the Pauli blocking in the final state between scattered nucleons. We accept the collision if this motion brings the two nucleons outside the two Fermi spheres, according to a probability corresponding to the level of *NN* collisions which are supposed to be really produced, in order to mimic the fact that in-medium effects can affect the number of allowed *NN* collisions. For each incident energy, we perform a run of 100 000 collisions in order to scan extensively the corresponding available phase space, and we vary the probability between 0 (no allowed collision) and 1 (fully allowed collisions given the available phase space) for each run. We then register the ratio $\mathcal{C}$ between accepted and attempted collisions for each value of the probability at a given incident energy. The obtained correlations between $\mathcal{C}$ and the stopping ratio $\mathcal{S}$ are displayed in Fig. 5 for incident energies between $30A$ and $110A$ MeV, each point corresponding to one probability value for a given incident energy.

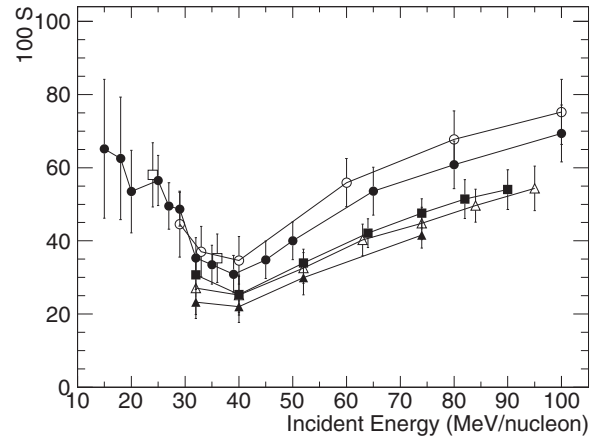

FIG. 4. Stopping ratio $\mathcal{S}$ (see text) as a function of incident energy. Symbols are the same as for Fig. 3.

This procedure accounts for the Pauli exclusion principle in p-space and allows us to compute the isotropy ratio R_E [Eq. (1)] and the stopping ratio $\mathcal{S}$ [Eq. (3)]. By varying the incident energy between $30A$ and $110A$ MeV, we find that $\mathcal{S}$ is related to the ratio of accepted *NN* collisions $\mathcal{C}$ by the following empirical formula as illustrated by the curves in Fig. 5:

$$\mathcal{C} \approx \mathcal{S}^{\beta(E_{\rm inc})} \tag{4}$$

with $\beta = 1.32$ at $E_{\rm inc} = 30A$ MeV, and $\beta = 0.74$ at $E_{\rm inc} = 110A$ MeV. The quality of this approximation is illustrated by the agreement between the fits (curves) and the symbols in Fig. 5. This is also quantified by the reduced χ^2 values in the inserted table. The energy dependence for β is then simply parametrized as a smooth quadratic dependence upon the incident energy in A MeV: $\beta(E_{\rm inc}) = 1.643 - 1.155\times10^{-2}E_{\rm inc} + 2.974\times10^{-5}E_{\rm inc}^2$. This parametrization nicely describes the correlation between $\mathcal{C}$ and $\mathcal{S}$ for the considered energy range with a good level of accuracy; it can be seen as the functional

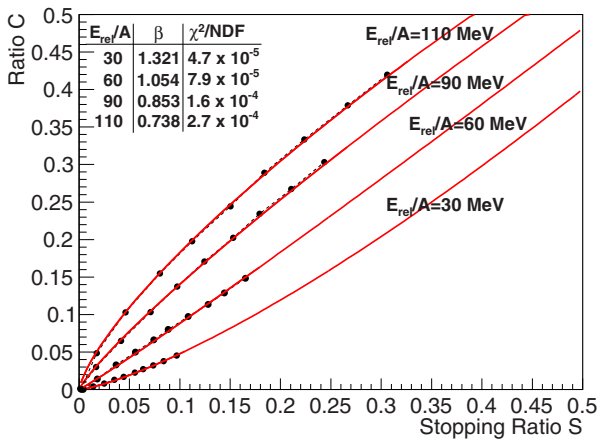

FIG. 5. (Color online) Correlation between the probability $\mathcal{C}$ of accepted collisions and the stopping ratio $\mathcal{S}$ for two Fermi spheres separated by relative energies of $30A$,$60A$,$90A$,$110A$ MeV (symbols). The curves correspond to the fits S^{β}, with the β values displayed in the inserted table and their corresponding reduced χ^2 values.

form between the stopping ratio $\mathcal{S}$ and the percentage of NN collisions $\mathcal{C}$ for the corresponding available phase space. In the following, we will use this quantity $\mathcal{C}$ calculated from Eq. (4) to extract information on NN collisions.

C. Mass scaling and characteristic length

To understand the mass hierarchy observed in Figs. 3 and 4, we scale the latter quantity $\mathcal{C}$ by $A_{\rm tot}^{\gamma}$, $A_{\rm tot}$ being the total mass number of the system, and γ varying between 1/4 and 2/3. The results are shown in Fig. 6. For $\gamma \approx \frac{1}{3}$, all experimental points collapse on a single curve for the whole range of incident energy and for all systems; the agreement is somehow particularly impressive for incident energies above the Fermi energy.

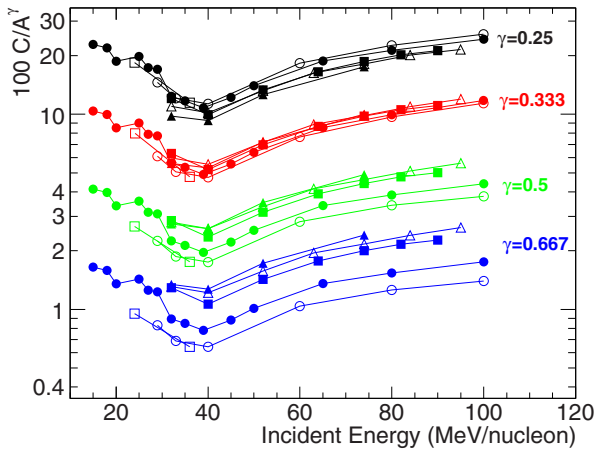

FIG. 6. (Color online) Scaled quantity $\mathcal{C}/A_{\rm tot}^{\gamma}$ (see text), here multiplied by 100, as a function of incident energy for $\gamma = 0.25$, 0.333,0.5,0.667. Symbols are the same as for Fig. 3.

This result suggests defining a characteristic quantity $A_{\rm tot}^{1/3}$, homogeneous to a length, connected to the radial extent of the system formed in central collisions. This length appears to be a key quantity for describing the amount of stopping and hence the percentage of NN collisions. In a *Glauber* picture, this can be seen as the *characteristic length* associated with NN collisions in nuclear matter. From this, we can infer that the corresponding reduced value $\mathcal{C}/A_{\rm tot}^{1/3}$ is related to the associated mean free path for NN collisions.

IV. IN-MEDIUM EFFECTS

A. Nucleon mean free path

In this section, we estimate the mean free path for a nucleon from the stopping ratio $\mathcal{S}$ and the related quantity $\mathcal{C}$. We postulate from the previous findings that the mean free path λ_{NN} can be simply expressed as the *inverse* of $\mathcal{C}$:

$$\lambda_{NN} \approx L/\mathcal{C}, \tag{5}$$

where L is a characteristic length proportional to $A_{\rm tot}^{1/3}$, taken equal to the average nuclear radius $L = r_0 A^{1/3}$ with $r_0 = 1.2$ fm and $A = A_{\rm tot}/2 \approx A_{\rm projectile} \approx A_{\rm target}$. L can be interpreted as a quantity related to the average distance traveled by a nucleon. Also, we assume implicitly that the quantity $\mathcal{C} = S^{\beta}$ corresponds to the percentage of NN collisions when the two incoming nuclei fully overlap in r-space, as one can expect for central collisions. At this stage, we do not expect any significant change for λ_{NN} if we consider a higher density ($\rho/\rho_0 \approx 1.2$), hence a slightly smaller L value, for the colliding system.

Applying Eq. (5), we plot the results in Fig. 7. We see that λ_{NN} is maximum around $E_{\rm inc} = 35A$–$40A$ MeV, thus corresponding to a minimum value for the stopping as observed in Figs. 3 and 4, and reaches $\lambda_{NN} = 9.5 \pm 2$ fm. This depicts the fact that the Pauli principle suppresses to a large extent NN collisions at low incident energy and consequently increases the mean free path around the Fermi energy [12]. The decrease observed at lower incident energy is here attributed to mean-field effects, for which the dissipation mechanism is mainly

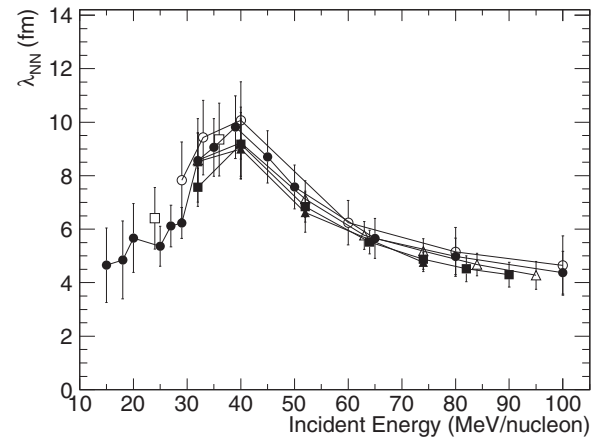

FIG. 7. Mean free path for a nucleon in nuclear matter as a function of incident energy. Symbols are the same as for Fig. 3.

provided by one-body rather than two-body dissipation. In this energy domain, the stopping ratio $\mathcal{S}$ (and consequently $\mathcal{C}$) should be certainly computed in a more appropriate way since the sudden approximation taken here as a reference for $\alpha = 1$ [no mean-field dissipation, see Eq. (2)] should be less valid. This will be extensively studied in a forthcoming paper.

If we now focus on the high energy domain, i.e., above the Fermi energy, we note a continuous decrease of λ_{NN}, whatever the system size, toward an asymptotic value corresponding to $\lambda_{NN} = 4.5 \pm 1$ fm above 100A MeV. These values are compatible with both experimental data [30,31] and recent theoretical studies [18] around and above 100A MeV. This agreement also suggests that the characteristic length L is indeed closely related to the nuclear radius of the colliding system and justifies *a posteriori* our assumption.

B. Nucleon-nucleon cross section

From our estimated mean free paths, we can now determine the in-medium nucleon-nucleon cross section by taking the standard formula from kinetic theory: $\sigma_{NN} \approx 1/(\rho\lambda_{NN})$. We choose here the density $\rho = 1.2\rho_0$ with $\rho_0 = 0.17$ fm^{-3} since we are looking at central collisions where the two nuclei are supposed to strongly overlap in r-space. The density value taken here is considered as a standard value concerning the incident energy range 30A–100A MeV [32]. We could have taken a more sophisticated energy-density dependence, but it would not affect the results as explained later on. We then obtain the values of σ_{NN} displayed in Fig. 8, with an asymptotic value at high energy close to 12 mb. This value is in full agreement with the work of [7], where elastic in-medium nucleon-nucleon cross sections have been obtained by the comparison between FOPI data and a relativistic Dirac-Brueckner transport model (see Fig. 3 in [7]). In the following, we will compare our extracted in-medium cross-sections to the free values in vacuum.

C. In-medium effects

To disentangle the different in-medium effects, we start by evaluating the Pauli blocking. Several methods can be

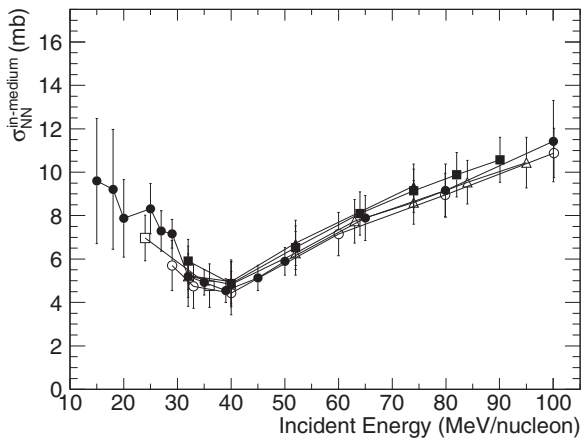

FIG. 8. In-medium nucleon-nucleon cross section as a function of incident energy for $\rho = 1.2\rho_0$ (see text). Symbols are the same as for Fig. 3.

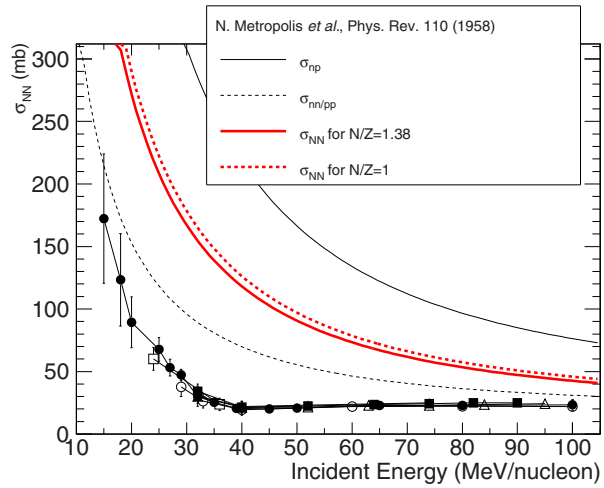

FIG. 9. (Color online) In-medium nucleon-nucleon cross section corrected from Pauli effects (see text) as a function of incident energy. The different curves correspond to the free values for nn/pp, np, and NN cross section for two isospin ratios $N/Z = 1$, 1.38. Symbols are the same as for Fig. 3.

employed [33,34]. We use in this study the simple prescription of Kikuchi and Kawai [35] where the probability P to perform a NN collision is given by

$$P(\zeta) = 1 - 7\zeta/5 \quad \text{for } \zeta \leqslant 0.5,$$
$$P(\zeta) = 1 - 7\zeta/5 + 2\zeta(2 - 1/\zeta)^{5/2}/5 \quad \text{for} \quad \zeta > 0.5,$$

with $\zeta = E_{\text{Fermi}}/(E_{\text{inc}} + E_{\text{Fermi}})$. E_{inc} is the incident energy between the two incoming nuclei, and $E_{\text{Fermi}} = 38(\rho/\rho_0)^{2/3}$ is the Fermi energy for a nucleus at density ρ. By dividing σ_{NN} as reported in Fig. 8 by $P(\zeta)$, we thus obtain nucleon-nucleon cross sections, out of Pauli effects, which have to be compared to the standard free values [36] as shown by Fig. 9.

The curves correspond to the values for neutron-neutron/proton-proton (nn/pp), neutron-proton (np), and a combination of both [29] to get σ_{NN} for a given nucleus with $N/Z = 1$, 1.38 (N/Z values corresponding to some of the systems studied here; see Table I). We observe that the experimental in-medium NN cross sections are systematically lower than the free cross sections, tending however to recover the free values at high incident energy, well above 100A MeV. This shows that additional in-medium effects, outside Pauli effects, are indeed present and have to be taken into account for renormalizing the free nucleon-nucleon cross sections in nuclear matter. Note, however, that we may have underestimated the Pauli blocking as it was determined only in p-space instead of the full phase space [33], but we do not expect that this could change drastically our findings.

To get more quantitative results, we compute the in-medium factor $\mathcal{F} = \sigma_{NN}^{\text{in-medium}}/\sigma_{NN}^{\text{free}}$ from Fig. 9. It is displayed in Fig. 10 where we restrict our discussion to the incident energy range 30A–100A MeV. As already discussed, the data could give nonphysical results at incident energy lower than the Fermi energy (shaded area in Fig. 10) and should not be taken into account in this comparison. For this specific energy range, we should apply a special treatment to the stopping ratio

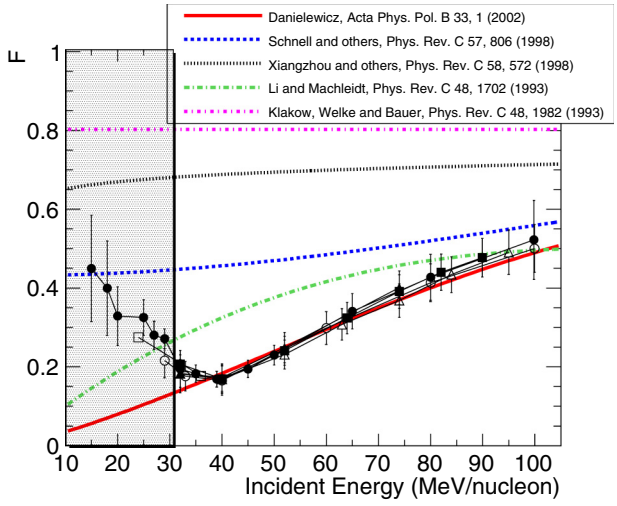

FIG. 10. (Color online) In-medium factor $\mathcal{F} = \sigma_{NN}^{\text{in-medium}}/\sigma_{NN}^{\text{free}}$ for the nucleon-nucleon cross section in nuclear matter. The different curves correspond to some parametrizations used in transport models. Symbols are the same as for Fig. 3.

$\mathcal{S}$, with mean-field effects properly evaluated, in order to be compared with theoretical prescriptions. These aspects will be studied in a forthcoming paper as already mentioned.

The reduction factor $\mathcal{F}$ strongly evolves with incident energy, between 0.2 and 0.5 for the incident energy range $35A$–$100A$ MeV. We also plot in Fig. 10 some parametrizations taken from recent works and currently used in transport models [15,37–40]. They give rather different results in the Fermi-energy domain, showing that $\sigma_{NN}^{\text{in-medium}}$ is poorly constrained at the present time. All theoretical prescriptions are density-dependent and can give different results when changing density, taken here at a fixed value $\rho = 1.2\rho_0$. Nevertheless, scanning the expected density values $\rho = 1$–$1.5\ \rho_0$ in this incident energy domain, we have observed for $\mathcal{F}$ only small differences of $\pm 10\%$, encompassed by the experimental error bars.

From this comparison, we see that the parametrization of the MSU group [40,41] is in excellent agreement—within the error bars—with our experimental findings. It is based upon the assumption that the geometric cross-section radius should not exceed the interparticle distance [40] and is implemented as

$$\sigma_{NN}^{\text{in-medium}} = \sigma_0 \tanh\left(\sigma_{NN}^{\text{free}}/\sigma_0\right), \quad \sigma_0 = y\rho^{-2/3}, \quad y = 0.85.$$

The other prescriptions are unable to reproduce the overall trend in the considered energy range, neither in shape nor in magnitude, except Schnell *et al.* [38] and Li *et* Machleidt [15] at the highest incident energies ($E_{\text{inc}} \geqslant 90A$–$100A$ MeV). We can conclude from this part that the medium (density) effects lead to a strong reduction of the NN cross section (by a factor between 2 and 5), and that their energy dependences have to be properly accounted in the range $E_{\text{inc}}/A = 35$–100 MeV.

V. CONCLUSIONS

We evaluated nuclear stopping from the measured isotropy ratio for protons in central collisions for a large body of symmetric systems studied with the INDRA array. We derived quantitative information on the in-medium transport properties in the Fermi-energy domain. First, we have found that the stopping is not complete above $E_{\text{inc}} = 30A$ MeV, whatever the system size. Second, we have shown that we can get consistent results by scaling the appropriate stopping ratio by the characteristic size of the system. We have then established a relation between the stopping ratio and the nucleon mean free path in nuclear matter. We found $\lambda_{NN} = 9.5 \pm 2$ fm at $E_{\text{inc}} = 40A$ MeV and $\lambda_{NN} = 4.5 \pm 1$ fm for $E_{\text{inc}} = 100A$ MeV, in agreement with theoretical predictions. We also estimated the in-medium effects for the nucleon-nucleon cross section by disentangling Pauli blocking effects from higher-order correlations due to density (many-body correlations) in nuclear matter. The best parametrization is the one provided by Danielewicz [40], which allows us to reproduce the experimental values extracted from this analysis. It is interesting to note that this parametrization has been established in a phenomenological way [40]. We conclude that in-medium effects are quite important since they give a significant reduction of the nucleon-nucleon cross section, namely 80% at $E_{\text{inc}} = 35A$ MeV and 50% at $E_{\text{inc}} = 100A$ MeV. This strong energy dependence for the in-medium nucleon-nucleon cross section has to be properly taken into account in any transport model based on the Boltzmann equation, where a two-body collision term is considered. As a perspective, the availability of radioactive beam facilities in the Fermi-energy domain could allow us to probe more deeply the isopin dependence of the mean free paths, nucleon-nucleon cross-sections, and also effective masses. In any case, this could provide valuable information about the isovector properties of the nuclear interaction in dense nuclear matter.

[1] A. Ohnishi and J. Randrup, Phys. Rev. Lett. **75**, 596 (1995).
[2] J. Aichelin, Phys. Rep. **202**, 233 (1991).
[3] A. Bonasera *et al.*, Phys. Rep. **243**, 1 (1994).
[4] P. Chomaz, M. Colonna, A. Guarnera, and J. Randrup, Phys. Rev. Lett. **73**, 3512 (1994).
[5] A. Ono, H. Horiuchi, T. Maruyama, and A. Ohnishi, Phys. Rev. Lett. **68**, 2898 (1992).
[6] W. Reisdorf *et al.*, Phys. Rev. Lett. **92**, 232301 (2004).
[7] T. Gaitanos *et al.*, Phys. Lett. B **609**, 241 (2005).
[8] S. Kumar, S. Kumar, and R. K. Puri, Phys. Rev. C **81**, 014601 (2010).
[9] C. Fuchs and H. H. Wolter, Eur. Phys. J. A **30**, 5 (2006), and references therein.
[10] J. M. Lattimer and M. Prakash, Science **304**, 536 (2004).
[11] G. Lehaut *et al.* (INDRA Collaboration), Phys. Rev. Lett. **104**, 232701 (2010).
[12] D. Durand, B. Tamain, and E. Suraud, *Nuclear Dynamics in the Nucleonic Regime* (Institute of Physics, New York, 2001), and references therein.
[13] J. Cugnon, Ann. Phys. (Paris) **11**, 201 (1996).
[14] J. Lukasik *et al.* (INDRA and ALADIN Collaborations), Phys. Lett. B **608**, 223 (2005).

[15] G. Q. Li and R. Machleidt, Phys. Rev. C **48**, 1702 (1993).
[16] T. Frick, H. Muther, A. Rios, A. Polls, and A. Ramos, Phys. Rev. C **71**, 014313 (2005).
[17] V. Soma and P. Bozek, Phys. Rev. C **78**, 054003 (2008).
[18] A. Rios and V. Soma, Phys. Rev. Lett. **108**, 012501 (2012).
[19] G. D. Westfall *et al.*, Phys. Rev. Lett. **71**, 1986 (1993).
[20] A. Andronic *et al.*, Eur. Phys. J. A **30**, 31 (2006), and references therein.
[21] J. Pouthas *et al.*, Nucl. Instum. Methods A **357**, 418 (1995).
[22] B. Borderie, J. Phys. G **28**, R217 (2002).
[23] E. Plagnol *et al.* (INDRA Collaboration), Phys. Rev. C **61**, 014606 (1999).
[24] V. Métivier *et al.* (INDRA Collaboration), Nucl. Phys. A **672**, 357 (2000).
[25] S. Hudan *et al.* (INDRA Collaboration), Phys. Rev. C **67**, 064613 (2003).
[26] J. Lukasik *et al.* (INDRA and ALADIN Collaborations), Phys. Rev. C **66**, 064606 (2002).
[27] A. Le Fevre *et al.* (INDRA and ALADIN Collaborations), Nucl. Phys. A **735**, 219 (2004).
[28] G. Q. Zhang *et al.*, Phys. Rev. C **84**, 034612 (2011).
[29] S. K. Charagi and S. K. Gupta, Phys. Rev. C **41**, 1610 (1990).
[30] P. U. Renberg, D. F. Measday, M. Pepin, P. Schwaller, B. Favier, and C. Richard-Serre, Nucl. Phys. A **183**, 81 (1972).
[31] A. Nadasen *et al.*, Phys. Rev. C **23**, 1023 (1981).
[32] P. Danielewicz, Phys. Rev. C **51**, 716 (1995).
[33] B. Chen, F. Sammarruca, and C. A. Bertulani, Phys. Rev. C **87**, 054616 (2013).
[34] J. Su and F.-S. Zhang, Phys. Rev. C **87**, 017602 (2013).
[35] K. Kikuchi and M. Kawai, *Nuclear Matter and Nuclear Collisions* (North Holland, New York, 1968).
[36] N. Metropolis *et al.*, Phys. Rev. **110**, 204 (1958).
[37] D. Klakow, G. Welke, and W. Bauer, Phys. Rev. C **48**, 1982 (1993).
[38] A. Schnell, G. Ropke, U. Lombardo, and H. J. Schulze, Phys. Rev. C **57**, 806 (1998).
[39] C. Xiangzhou, F. Jun, S. Wenqing, M. Yugang, W. Jiansong, and Y. Wei, Phys. Rev. C **58**, 572 (1998).
[40] P. Danielewicz, Acta. Phys. Pol. B **33**, 45 (2002).
[41] D. D. S. Coupland, W. G. Lynch, M. B. Tsang, P. Danielewicz, and Y. Zhang, Phys. Rev. C **84**, 054603 (2011).